In: European Radar Conference (EuRAD) 2021, 5-7 April 2022, London, UK. pp. 114-117
DOI: 10.23919/EuRAD50154.2022.9784488

Realistic Simulation of Drone Micro-Doppler Signatures

Cameron Bennett[#*1], Stephen Harman[#2], Ivan Petrunin[*3]

[#]Aveillant Ltd, Cambridge, UK

[*]Cranfield University, UK

{[1]cameron.bennett, [2]stephen.harman}@aveillant.com, [3]i.petrunin@cranfield.ac.uk

***Abstract* — This paper presents a novel approach to simulating micro-Doppler signatures caused by drones. The focus of this work is to produce realistic signatures that represent the variation that is observed in live radar measurements. In order to accomplish this, the kinematics and dynamics of a drone flight are modelled to capture the changing rotor rotation rates. The simulation results show realistic variation that is representative of measured drone flights.**

***Keywords* — Unmanned aerial vehicles; Radar detection; Micro-Doppler; Simulation; Staring radar.**

I. Introduction

The increased presence of drones in civil airspace has led to a demand for more robust recognition techniques in radars. Micro-Doppler signatures caused by the rotating propellers on drones have been shown to provide promising discrimination between drones and other targets, particularly when adopted as part of deep learning architectures [[1][2]]. However, access to radar measurements of drones flying in live environments is limited and this can hinder the performance of classification models. Simulations of the micro-Doppler signatures can offer a means of replacing or preferably supplementing datasets of measured drone flights.

The theory behind micro-Doppler signatures from rotating propellers has been researched for many decades due to its overlap with modelling Jet Engine Modulation (JEM) and HElicopter Rotor Modulation (HERM) lines observed from aircraft. The theoretical time signal from an aircraft propeller has been is established in [3] and has been widely adopted in following research. Several papers have expanded upon this model and applied it to different target types. In [4], the model is expanded to account for the contributions from the face of the propellers and represent the blades as rectangular flat plates. In [5], this model is simulated and validated with measured signals from a W-band radar for small rotary-winged drones. [6], [7] also validate this model at lower frequencies in S-band and X-band and in [8], a similar model is validated with a staring radar.

The variation in propeller RPM(Revolutions Per Minute) during a drone flight significantly impacts the micro-Doppler signatures observed by the radar. Micro-Doppler components are observed from the approaching and receding edges of propeller blades and so the signatures mirror the RPM of the rotors on the drone. Simulations with fixed RPM applied to the rotors result in noticeably synthetic signatures which have perfect, static displacement of the micro-Doppler components around the main body component. The current literature lacks any simulation models that represent the variation in micro-Doppler components seen in measured drone signatures.

In order to accurately represent the variation and trends in measured drone signatures, a kinematic model was developed during this research. This model determines the rotation frequencies of each of the propellers based on a drone's trajectory and this provides realistic variation in the simulated signatures that is representative of measured data. Figure 1 contains an overview of the processing stages in the proposed simulator. A trajectory is defined at its input (simulated or GPS) and the kinematics and dynamics simulator uses this information to calculate the required RPM of each of the rotors to follow this trajectory. The positions of the rotors at each time frame are then fed into the scattering simulator which simulates the radar backscatter from the rotor blades. The combination of a dynamics and electromagnetic model provides a key novel contribution that results in simulation results with realistic variations.

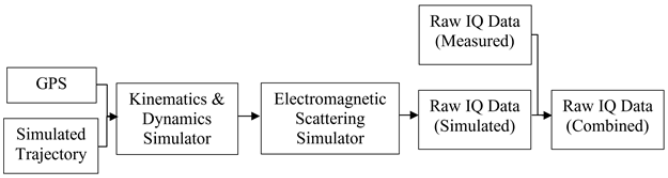

Figure 1: Overview of proposed micro-Doppler simulator.

II. Rotating Scatterer Model

A single rotating point scatterer can be simulated by a waveform with a time-varying Doppler shift. The phase modulation can be modelled by tracking the range of the scatterer from the radar as has been demonstrated in [7]. A scatterer rotating around a fixed point is illustrated in Figure 2.

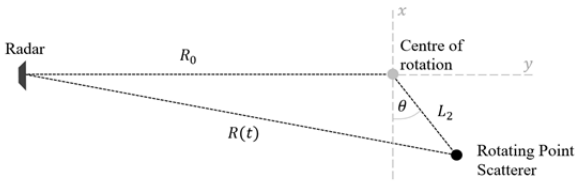

Figure 2: Illustration of a rotating scatterer

In Figure 2, R_0 is the range of the centre of rotation from the radar. In this case, the centre of rotation would be the one of the drone's rotors. $R(t)$ is the time varying range of the

© 2022 IEEE. Personal use of this material is permitted. Permission from IEEE must be obtained for all other uses, in any current or future media, including reprinting/republishing this material for advertising or promotional purposes, creating new collective works, for resale or redistribution to servers or lists, or reuse of any copyrighted component of this work in other works

rotating scatterer, θ is the angle between the plane of rotation and the x-axis and L_2 is the radius of the point scatterer's rotation. The backscatter from a rotating point scatterer can be modelled as a phase modulated waveform. The contribution from each point scatterer can be integrated along the length of a rotor blade to give an expression for the backscatter from the full blade [3], [7], [9]

$$s(t) = \int_{L_1}^{L_2} e^{j(2\pi f_c t - \frac{4\pi}{\lambda}(R_0 + vt + \cos(\beta) L \sin(\theta(t))))}\, dL \quad (1)$$

$$= (L_2 - L_1)\, sinc\left(\frac{2\pi(L_2 - L_1)}{\lambda}\left(cos(\beta)\, sin\big(\theta(t)\big)\right)\right) \times e^{j(2\pi f_c t - \frac{4\pi}{\lambda}(R_0 + vt + \frac{L_2 + L_1}{2}\cos(\beta)\, \sin(\theta(t))))}$$

where β is the angle between the radar's line of sight to the target and the rotating scatterer's plane of rotation, v is the target's range rate and L_1 is the distance from the centre of rotation to the blade root.

In practice, rotor blades are designed with twist and their density is unevenly spread across the length of the blade. Figure 3 shows a DJI Inspire propeller that has a large width close to the centre of rotation which decreases as it extends from the centre of rotation. The pitch also decreases towards the edges of the blade. The uneven shape of the propellers causes dense portions of the blade to backscatter with a greater intensity than those thinner portions at the edges. In order to account for this and allow for different types of blade, a discrete version of **Error! Reference source not found.** was adopted with a weighting function, *A,* which is custom defined depending on the modelled blade and normalised. The total backscattered signal at each timestep from all blades and rotors is defined as

$$S(t) = \sum_{r=1}^{N} \sum_{b=1}^{B} \sum_{L=L1}^{L2} A(L) e^{j(2\pi f_c t - \frac{4\pi}{\lambda}(R_r(t) + vt + L cos(\beta(t))\, sin(\theta_{r,b}(t))))} \quad (2)$$

where B is the number of blades on each rotor and N is the number of rotors on the drone.

Figure 3: Example of variation in pitch and width of propellers. DJI Inspire propellers[10].

III. Rotary Drone Kinematics and Dynamics Model

The following section outlines a simplified model of a rotary-winged drone's dynamics. This is aimed at representing the variation in rotor RPM that is reflected in micro-Doppler signatures. It is not intended to represent the intricate rotor control that would result from closed-loop feedback in live drone flights although additive Gaussian noise is included to represent this behaviour. The thrust required by each rotor during the flight is calculated incrementally by considering vertical, horizontal and rotational motion in succession. Figure 4 contains a high-level overview of the processing steps involved in this model. The remainder of this section will briefly describe each of the processing steps.

Algorithm 1: Pseudocode for Kinematics and Dynamics Model.

```
model KinematicsAndDynamics (s);
Input  : Trajectory path of drone DroneTraj.
Output: Rotor Frequencies, Rotor Positions, Pitch, Incident Angles.
Extract the XYZ velocity and acceleration from DroneTraj;
Extract the yaw at each timestep using the heading;
for timeFrame in DroneTraj do
    Calculate required horizontal and vertical forces from
     acceleration;
    Calculate thrust required on each rotor to meet vertical
     force;
    Adjust pitch of drone to meet horizontal force by
     changing relative thrust of the front and rear rotors;
    Calculate required angular acceleration in yaw axis;
    Adjust clockwise/anticlockwise pairs of rotors to meet
     angular acceleration;
    Convert thrust for each rotor to rotor frequency and save
     to an array for this timestep;
    Rotate the drone (update rotor positions and pitch);
    Calculate the incident angle at this timestep;
end
Add Gaussian noise to rotor frequencies with standard
  deviation proportional to RPM;
```

Figure 4: High level overview of processing steps involved in kinematics and dynamics model.

A. Initialisation

The initialisation of the drone simulation sets the foundation for all calculations in the kinematics/dynamics model. Rotary drones require balanced positioning of propellers to stabilise the drone during flight and when hovering. This means that the rotors are positioned equidistantly around the centre of mass. Realistic placement of the rotors is important as it prevents constructive and destructive interference between the backscatter of each rotor and impacts the resulting tilt caused by rotor thrust. The initial angle of the blades, θ, is also randomised to avoid unnatural interference effects. The rotors are required to rotate in alternate directions which avoids an undesirable net torque caused by the rotating propellers acting on the overall movement of the drone. Therefore, the rotors are assigned clockwise or anti-clockwise directions during initialisation.

Following initialisation of the drone, the input trajectory is analysed and the XYZ velocity and acceleration are extracted. The heading at each timestep is also calculated and used to determine the yaw of the drone. These values are necessary for the subsequent dynamics simulations.

B. Dynamics

Figure 5 contains a diagram that illustrates the resolved horizontal and vertical forces of a drone that is tilted at a pitch, θ. The resolved forces can be used to extract the thrust that is required to match the vertical and horizontal accelerations defined by the input trajectory.

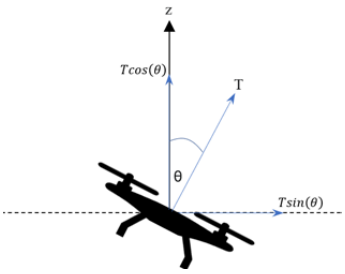

Figure 5: A diagram illustrating the direction that the thrust from the drone's rotors acts in and the resolved horizontal and vertical forces.

1) Vertical Motion

Vertical acceleration is the most fundamental movement of a rotary-winged drone. To accelerate in this plane, a drone simply requires the thrust from all rotors to increase or decrease at the same rate. The thrust required on each rotor to maintain the required height can be calculated as

$$F_z = m(a_z + g), \qquad T_z = \frac{F_z}{Rcos(\theta)} \tag{2}$$

where F_z, is the vertical force required to maintain the input trajectory, T_z is the thrust required to meet the vertical force and R, is the number of rotors.

2) Horizontal Motion

Horizontal motion in a rotary-winged drone is caused by tilting in a particular direction which increases the resolved horizontal force. By changing the relative thrust of the rotors, a net torque is applied to the drone's body causing it to tilt. In the simulation, the front and rear rotors are adjusted to create enough torque to achieve the required pitch. This results in an increased horizontal force that propels the drone forward.

3) Yaw Rotation

Control of the drone's yaw is a result of the net torque acting on the drone from all the rotors. Updates to the yaw in the simulator take advantage of the fact that the net torque acting on the yaw axis of the body is the difference of the torque resulting from the clockwise and counter-clockwise rotors. The necessary torque is calculated from the acceleration in the yaw of the input trajectory. The torque on each rotor is increased or decreased to match the required acceleration in yaw.

4) Drag

There are two components of drag acting on the drone at any given moment. These are the linear drag caused by the body's linear velocity between two points and the angular drag from the angular velocity of the drone as it tilts. The linear drag and angular drag used are defined in [11]. The rotor thrusts are then converted into rotor frequencies using the relationships defined in [12], [13].

C. Practical limits and environmental considerations

In a live environment, there are several physical limitations and external influences that impact the rotation frequencies of the drone's propellers. The physical limitations include maximum constraints on pitch, RPM, angular velocities, and horizontal velocities and these have been incorporated into the model[10]. External influences such as wind will also impact the rotor frequencies. Variations from the closed loop feedback system in the drone will result in rapid changes in RPM as the control system attempts to stabilise the drone. These fluctuations result in the magnitude of the micro-Doppler components being spread in frequency. Without these fluctuations, the energy is condensed into a sharp peak in the spectrum that is not representative of measured signatures. Therefore, Gaussian noise with a standard deviation that is proportional to the rotation frequency is added to the rotor frequencies in the kinematic model.

IV. Experimental and Simulated Data

As part of this work, a DJI Inspire drone was measured using Aveillant's Gamekeeper 16U Radar. The measured flight path was used as the trajectory from which micro-Doppler signatures were simulated so that the output could be directly compared with measured data. All parameters used in the simulation were based on the specification of the DJI Inspire I [10] to replicate the signatures as accurately as possible.

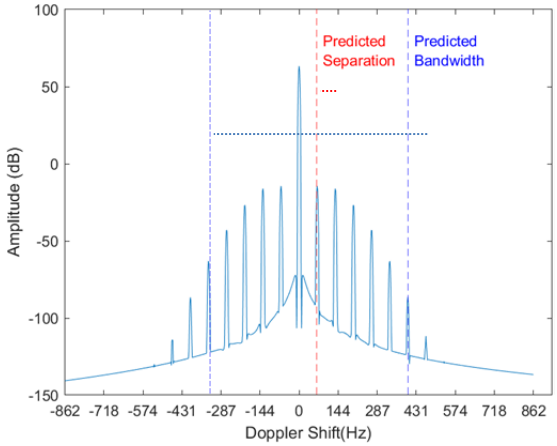

Figure 6: Spectrum of simulated signature with predicted separation between micro-Doppler components(red) and predicted bandwidth of significant sidebands (blue) as defined in [3]. NoRotors=1, Blade length=23cm, RPM=2000, NoBlades=2, θ=0, λ=23.9cm.

In Figure 6, the spectrum from a simulated flight with fixed parameters (RPM, position, pitch) is shown. The anticipated separation between components and bandwidth of the significant sidebands defined in [3] are highlighted. The spectrum aligns closely with these values and contains 6 significant sidebands which also aligns with findings in [3]. Figure 7 contains a spectrogram from a simulated signature based on measured GPS data. The Doppler components show realistic variations from the varying range rate and constantly changing rotor RPMs. The spectrogram of the measured flight is included in this figure for direct comparison. As the drone accelerates, the difference in RPM between the front and rear rotors begins to increase and this can be seen in both the simulated and measured spectrograms. In the first portion of the flight where the range rate is 0, the drone is ascending to

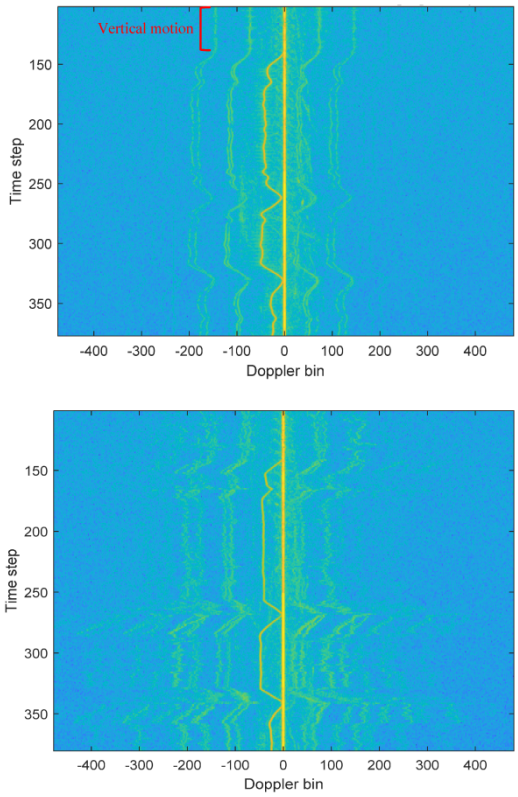

Figure 7: Spectrograms of simulated (Top) and measured (Bottom) drone flights. 1 Doppler bin = 1.79Hz.

its first waypoint. This portion of the flight is mostly vertical motion so the micro-Doppler components are narrowly spaced without large variations between the rotor speeds. There are slight deviations due to small changes in yaw and horizontal movement which occasionally disperses the energy across multiple doppler bins. As the drone tilts and accelerates horizontally, the difference in the back and front rotors causes the HERM lines to split in two.

The frequencies of the HERM lines in the measured and simulated signatures are constrained to within 5.4Hz throughout the spectrogram. The trends in simulated rotor speeds align well with the variation observed in measured signatures. The graph in Figure 8 shows that the average Doppler bin of the first micro-Doppler component has a similar trend in the simulated and measured spectrograms. The most noticeable difference between the signatures is that the measured data contains more activity at higher harmonics. These harmonics can be faintly seen above the noise in the simulated signatures however they are more prominent in the measured signals. This is likely due to the accuracy of the RCS characterisation of the blades in the model.

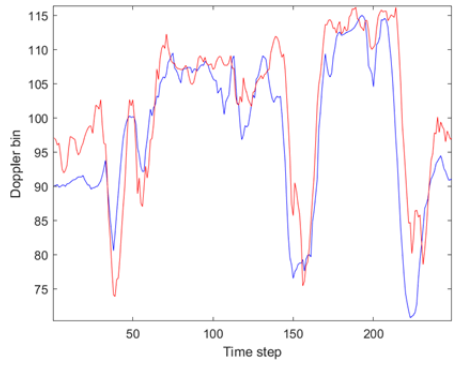

Figure 8: Average Doppler bin of first micro-Doppler cluster for the measured signature (red) and simulated signature (blue).

V. Conclusion

This paper has presented a novel approach to simulating micro-Doppler signatures caused by rotary-winged drones. By accounting for the dynamics of the drone, its rotor frequencies can be simulated which results in realistic variations in the micro-doppler signatures that are representative of measured radar signatures. The combination of the dynamics model and micro-Doppler signatures is the key novelty provided by this research. Having demonstrated promising results in this paper, there are further developments that will be explored in future work. In the kinematics model, Gaussian noise is used to represent the unpredictable variations in rotor frequency. However, a more refined model will be developed that accounts for the overall motion of the drone due to gusts of wind and the behaviour of rotors to counteract this. In addition, the drone's rotor speeds will be measured during a flight to gain a better understanding of their variation.

References

[1] C. Bennett, "An Investigation into Non-Cooperative Drone Classification in 3-D Staring Radars," University of Glasgow, 2019.

[2] D. A. Brooks, O. Schwander, F. Barbaresco, J. Y. Schneider, and M. Cord, "Temporal deep learning for drone micro-doppler classification," Proc. Int. Radar Symp., vol. 2018-June, doi: 10.23919/IRS.2018.8447963.

[3] J. Martin and B. Mulgrew, "Analysis of the theoretical radar return signal form aircraft propeller blades," in IEEE International Conference on Radar, May 1990, pp. 569–572, doi: 10.1109/RADAR.1990.201091.

[4] R. Melino, C. Bourne, and H. Tran, "Modelling Helicopter Radar Backscatter," 2011.

[5] S. Rahman and D. A. Robertson, "Radar micro-Doppler signatures of drones and birds at K-band and W-band," Sci. Rep., vol. 8, no. 1, pp. 1–11, 2018, doi: 10.1038/s41598-018-35880-9.

[6] J. J. M. De Wit, R. I. A. Harmanny, and G. Prémel-Cabic, "Micro-Doppler analysis of small UAVs," Eur. Microw. Week 2012 "sp. Microwaves", 9th Eur. Radar Conf. EuRAD 2012, pp. 210–213.

[7] J. Markow and A. Balleri, "Examination of Drone Micro-Doppler and JEM / HERM Signatures," no. D, pp. 0–5, 2020.

[8] S. Harman, "Characteristics of the Radar signature of multi-rotor UAVs," in 2016 European Radar Conference, Oct. 2016, pp. 93–96.

[9] V. C. Chen, F. Li, S.-. Ho, and H. Wechsler, "Micro-Doppler effect in radar: phenomenon, model, and simulation study," IEEE Trans. Aerosp. Electron. Syst., vol. 42, no. 1, pp. 2–21, Jan. 2006, doi: 10.1109/TAES.2006.1603402.

[10] DJI, "DJI Inspire I." https://www.dji.com/uk/inspire-1/ (accessed Nov. 2020).

[11] J. Taylor, Classical mechanics. University Science Books, 2005.

[12] R. W. Deters, S. Kleinke, and M. S. Selig, "Static testing of propulsion elements for small multirotor unmanned aerial vehicles," 35th AIAA Appl. Aerodyn. Conf. 2017, no. June 2018, 2017, doi: 10.2514/6.2017-3743.

[13] J. Brandt, R. Deters, G. Ananda, and M. Selig, "UIUC Propeller Database, University of Illinois.", https://m-selig.ae.illinois.edu/props/propDB.html.

https://dspace.org/

Realistic simulation of drone micro-Doppler signatures

Bennett, Cameron; Harman, Stephen; Petrunin, Ivan

2022-06-02
IEEE
https://doi.org/10.23919/EuRAD50154.2022.9784488
Bennett C, Harman S & Petrunin I (2022) Realistic simulation of drone micro-Doppler signatures. In: European Radar Conference (EuRAD) 2021, 5-7 April 2022, London, UK, pp. 114-117

Downloaded from a DSpace repository. https://dspace.org/